

# Interaction of a Néel-type skyrmion and a superconducting vortex

E. S. Andriyakhina<sup>1,2</sup> and I. S. Burmistrov<sup>2,3</sup>

<sup>1</sup>*Moscow Institute for Physics and Technology, 141700 Moscow, Russia*

<sup>2</sup>*L. D. Landau Institute for Theoretical Physics, acad. Semenova av. 1-a, 142432 Chernogolovka, Russia*

<sup>3</sup>*Laboratory for Condensed Matter Physics, HSE University, 101000 Moscow, Russia*

(Dated: December 23, 2024)

Superconductor–ferromagnet heterostructures hosting vortices and skyrmions are new area of an interplay between superconductivity and magnetism. We study an interaction of a Néel-type skyrmion and a Pearl vortex in thin heterostructures due to stray fields. Surprisingly, we find that it can be energetically favorable for the Pearl vortex to be situated at some nonzero distance from the center of the Néel-type skyrmion. The presence of a vortex–antivortex pair is found to result in increase of the skyrmion radius. Our theory predicts that a spontaneous generation of a vortex–anti-vortex pair is possible under some conditions in the presence of a Néel-type skyrmion.

## I. INTRODUCTION

Topological objects have been remaining at the focus of theoretical and experimental research for more than half a century. The existence of topologically stable configurations in ferromagnets with Dzyaloshinskii–Moriya interaction has been predicted by Bogdanov and Yablonskii [1]. Now these topological excitations, termed as skyrmions, are intensively explored in an emergent field of *skyrmionics* [2].

Research on an interplay between magnetism and superconductivity in heterostructures has long history [3–7]. Recently superconductor–ferromagnet bilayers hosting skyrmions have attracted great theoretical interest. It was understood that skyrmions in proximity with a superconductor can not only induce Yu–Shiba–Rusinov-type bound states [8, 9] but can also host Majorana modes [10–16]. It was found [17] that the presence of skyrmions affects strongly Josephson current via superconductor–ferromagnet–superconductor junction. It has been also shown [18] that skyrmion configurations can be stabilized by a superconducting dot or antidot situated at the top of a ferromagnetic film. In ferromagnet–superconductor heterostructures superconducting vortices and skyrmions can form bound pairs either due to interplay of proximity effect and spin-orbit coupling [19, 20] or due to their interaction via stray fields [21–23].

In this paper we study the interaction between a Néel-type skyrmion and a superconducting vortex in a chiral ferromagnet–superconductor heterostructure, see Fig. 1. We assume that the proximity effect is suppressed by the presence of a thin insulating layer between ferromagnet and superconductor such that the interaction between a skyrmion and a vortex is due to stray fields only. At first, by solving Maxwell–London equation we determine the Meissner current induced by a Néel-type skyrmion in the superconductor. Contrary to the previous work [23], we consider the case of ferromagnet and superconducting films of arbitrary widths. Analysis of the general expression, cf. Eq. (6), in the case of thin ferromagnetic and superconducting films yields that the supercurrent

has a maximum at distance of the order of the skyrmion size from the center of the skyrmion. Secondly, for thin ferromagnetic and superconducting films we compute the interaction energy between a Néel-type skyrmion and a Pearl vortex due to stray fields. Contrary to previous results, see Refs. [21–23], we find that in the case of a Néel-type skyrmion with the positive and negative chiralities it can be energetically favorable for a vortex to settle at some distance from the skyrmion’s center. At third, we study the effect of the presence of superconducting vortex–anti-vortex pair on the skyrmion size in thin heterostructures. We find that a Pearl vortex leads to increase of a skyrmion radius. Under some conditions, the spontaneous generation of a vortex–anti-vortex pair in a superconducting film is possible in the presence of a skyrmion.

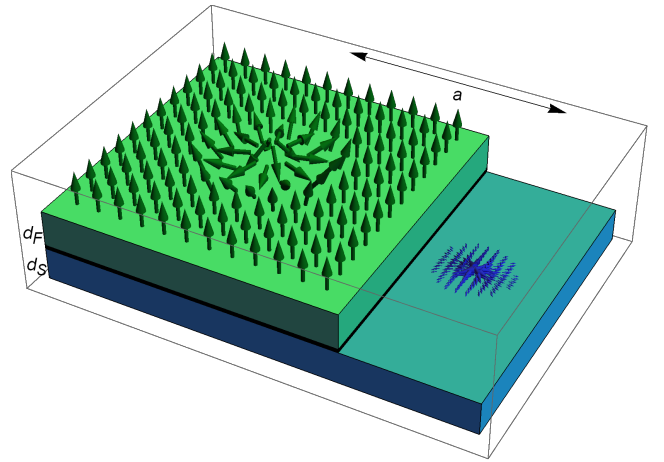


FIG. 1. Sketch of a ferromagnet (green) – superconductor (blue) bilayer. There is a thin insulating layer (black) which suppresses the proximity effect. The ferromagnetic layer hosts a Néel-type skyrmion. The magnetic profile of the skyrmion with the positive chirality is schematically shown. The superconducting layer hosts a vortex at some distance from the skyrmion’s center. The vortex is shown schematically by blue lines.  $d_F$  and  $d_S$  denote the width of the ferromagnet and superconductor film, respectively (see text).

The outline of the paper is as follows. In Sec. II the solution of the Maxwell–London equation is presented, and the results for the supercurrent are given. The interaction energy between a Néel–type skyrmion and a Pearl vortex is computed and analyzed in Sec. III. In Sec. IV the effect of a Pearl vortex on the skyrmion radius is estimated. We end the paper with summary and conclusions in Sec. V. Some technical details of computations are presented in Appendix.

## II. SUPERCURRENT GENERATED BY A NÉEL–TYPE SKYRMION

We start from calculation of the supercurrent in the chiral ferromagnet – superconductor heterostructure which is generated by a Néel–type skyrmion (see Fig. 1). The width of the chiral ferromagnet (superconductor) film is  $d_F$  ( $d_S$ ). We assume the presence of a thin insulating layer between the chiral ferromagnet and the superconductor that allows us to neglect the proximity effect. The magnetization profile of a Néel–type skyrmion in the chiral ferromagnet film in the cylindrical coordinate system with the origin at the center of the skyrmion is given as follows [24]

$$\mathbf{M}_{\text{Sk}} = M_s \Theta(z) \Theta(d_F - z) \left[ \mathbf{e}_r \eta \sin \theta(r) + \mathbf{e}_z \cos \theta(r) \right]. \quad (1)$$

Here  $\eta = \pm 1$  denotes the chirality of the skyrmion,  $M_s$  is the saturation magnetization of the chiral ferromagnet film, and  $\mathbf{e}_r$  and  $\mathbf{e}_z$  are unit vectors along the radial direction and the  $z$ -axis (perpendicular to the interface), respectively.

The spatial distribution of the vector potential  $\mathbf{A}_{\text{Sk}}$  is governed by the Maxwell–London equation:

$$\nabla \times (\nabla \times \mathbf{A}_{\text{Sk}}) + \Theta(-z) \Theta(z+d_S) \frac{\mathbf{A}_{\text{Sk}}}{\lambda_L^2} = 4\pi \nabla \times \mathbf{M}_{\text{Sk}}, \quad (2)$$

where  $\lambda_L$  stands for the London penetration depth. The Maxwell–London equation should be supplemented by the boundary conditions of continuity of  $\mathbf{A}_{\text{Sk}}$  and  $\partial \mathbf{A}_{\text{Sk}} / \partial z$  at  $z = -d_S, 0, d_F$  [25].

Since the right hand side of Eq. (2) is proportional to the unit vector  $\mathbf{e}_\varphi$ , the vector potential  $\mathbf{A}_{\text{Sk}}$  has only the azimuthal component  $A_{\text{Sk},\varphi}$  that depends on  $r$  and  $z$ . The solution for  $A_{\text{Sk},\varphi}(r, z)$  can be cast in the following form

$$A_{\text{Sk},\varphi}(r, z) = - \int_0^\infty dq J_1(qr) \frac{G(q)}{q} \times \begin{cases} \varkappa_2^V e^{-qz}, & z \geq d_F, \\ 1 + \varkappa_1^F e^{qz} + \varkappa_2^F e^{-qz}, & d_F > z \geq 0, \\ \varkappa_1^S e^{Qz} + \varkappa_2^S e^{-Qz}, & 0 > z \geq -d_S, \\ \varkappa_1^V e^{qz}, & -d_S > z, \end{cases} \quad (3)$$

where  $J_1(z)$  stands for the Bessel function of the first kind. Also we introduced  $Q = \sqrt{q^2 + 1/\lambda_L^2}$  and the function

$$G(q) = -4\pi M_s \int_0^\infty dr r J_1(qr) \theta'(r) \sin \theta(r). \quad (4)$$

Using the continuity of the azimuthal component of the vector potential,  $A_{\text{Sk},\varphi}$ , and its derivative,  $\partial A_{\text{Sk},\varphi} / \partial z$ , at  $z = -d_S, 0, d_F$ , we obtain

$$\begin{aligned} \varkappa_2^V &= \frac{1}{2} (e^{qd_F} - 1) - \lambda_L^{-2} \sinh(Qd_S) \mathcal{X}, \quad \varkappa_1^V = 2Q e^{qd_S} \mathcal{X}, \\ \varkappa_1^F &= -e^{-qd_F}/2, \quad \varkappa_2^F = -1/2 - \lambda_L^{-2} \sinh(Qd_S) \mathcal{X}, \\ \varkappa_1^S &= (Q + q) e^{Qd_S} \mathcal{X}, \quad \varkappa_2^S = (Q - q) e^{-Qd_S} \mathcal{X}, \\ \mathcal{X} &= \frac{q(1 - e^{-qd_F})}{(Q + q)^2 e^{Qd_S} - (Q - q)^2 e^{-Qd_S}}. \end{aligned} \quad (5)$$

The current density in the superconducting film, i.e. at  $-d_S \leq z \leq 0$ , can be calculated by means of the London equation,  $\mathbf{j} = -\mathbf{A}_{\text{Sk}} / (4\pi \lambda_L^2)$ . It is more convenient to trace the total supercurrent flowing in the superconducting film,  $J_\varphi(r) = \int_{-d_S}^0 dz j_\varphi(r, z)$ . Then, we retrieve

$$J_\varphi = \int_0^\infty dq \frac{J_1(qr)}{4\pi \lambda_L^2} \frac{G(q)(1 - e^{-qd_F})(1 - e^{-Qd_S})}{Q[q + Q - (Q - q)e^{-Qd_S}]} \quad (6)$$

We mention that this expression is similar to the expression for the current induced by a domain wall [26]. In the limit of a thick superconductor,  $d_S \gg \lambda_L, R$ , Eq. (6) transforms into the result of Ref. [23].

Below we shall focus on the case of a thin chiral ferromagnet,  $d_F \ll R$ , and a thin superconducting film,  $d_S \ll \lambda_L, R$ . As we shall demonstrate in the next section, the asymptotic behavior of the supercurrent can be found for an arbitrary smooth skyrmion profile with  $\theta(0) = \pi$  and  $\theta(r \rightarrow \infty) \rightarrow 0$ . Commonly used variational examples with such kind behavior are the exponential ansatz  $\theta(r) = \bar{\theta}(r/R)$  where  $\bar{\theta}(x) = \pi \exp(-x)$  and the 360-degree domain wall ansatz  $\bar{\theta}(x) = 2 \arctan(\sinh(R/\delta)/\sinh(Rx/\delta))$ . Also we shall consider the linear ansatz with  $\theta(r) = \pi(1 - r/R)$  for  $r < R$  and zero otherwise.

### A. The case of a smooth skyrmion profile

The behavior of the supercurrent with the distance from the center of the skyrmion is controlled by the function  $G(q)$ , see Eq. (4). It is convenient to introduce the dimensionless function,  $g$ , such that

$$\begin{aligned} G(q) &= 4\pi M_s R g(qR), \\ g(y) &= - \int_0^\infty dx x J_1(yx) \bar{\theta}'(x) \sin \bar{\theta}(x). \end{aligned} \quad (7)$$

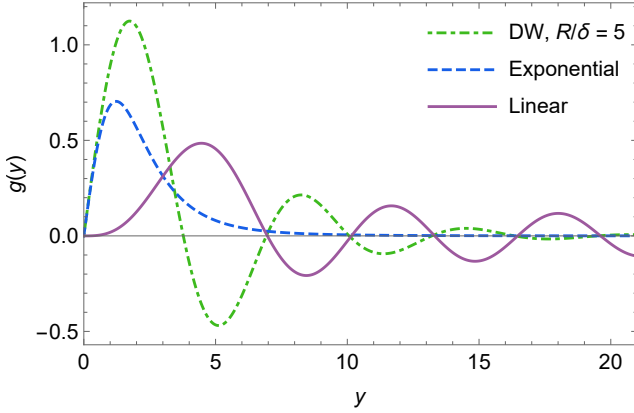


FIG. 2. The function  $g(y)$  in the cases of the exponential, domain wall and linear anzats.

Then in the case of a thin superconducting film,  $d_S \ll \lambda_L, R$ , and a thin chiral ferromagnet,  $d_F \ll R$ , Eq. (6) can be drastically simplified,

$$J_\varphi = M_s \frac{d_F}{R} \int_0^\infty dy \frac{yg(y)J_1(yr/R)}{1 + 2y\lambda/R}. \quad (8)$$

Here  $\lambda = \lambda_L^2/d_S$  denotes the Pearl penetration length [27]. The asymptotic behavior of the function  $g(y)$  is given as (see Appendix A),

$$g(y) = \begin{cases} 2c_2y & , \quad y \ll 1, \\ -9\bar{\theta}'(0)\bar{\theta}''(0)/(2y^4) & , \quad y \gg 1, \end{cases} \quad (9)$$

where we introduced the numerical constants

$$c_k = -\frac{1}{4} \int_0^\infty dx x^k \bar{\theta}'(x) \sin \bar{\theta}(x), \quad k = -1, 0, 1, \dots \quad (10)$$

For example, in the case of the exponential ansatz one finds  $c_2 \approx 0.51$ . The dependence of the function  $g(y)$  on  $y$  is shown in Fig. 2.

Let us first consider the case of the skyrmion size much smaller than the size of the vortex,  $R \ll \lambda$ . Evaluating the integral over  $q$  in Eq. (8), we obtain asymptotic behavior of the supercurrent (see Appendix A),

$$J_\varphi = \frac{M_s d_F}{\lambda} \begin{cases} c_{-1}r/R, & r \ll R, \\ c_2 R^2/r^2, & R \ll r \ll \lambda, \\ 12c_2 \lambda^2 R^2/r^4, & \lambda \ll r. \end{cases} \quad (11)$$

For  $\bar{\theta}(x) = \pi \exp(-x)$  one finds  $c_{-1} \approx 1.17$ . The asymptotic expression (11) suggests nonmonotonous spatial dependence of the supercurrent with a maximum at the distance of order of the skyrmion size  $R$  (see Fig. 3).

In the case of large skyrmion and small Pearl penetration length,  $R \gg \lambda$ , the supercurrent can be found to the lowest order in  $\lambda/R$  as (see Appendix A),

$$J_\varphi = -M_s \frac{d_F}{R} \bar{\theta}'(r/R) \sin \bar{\theta}(r/R). \quad (12)$$

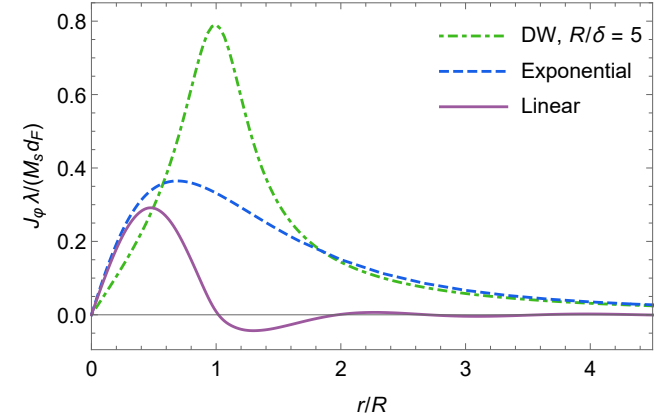


FIG. 3. The dependence of the supercurrent on the distance from the skyrmion center for  $d_S/\lambda_L = 0.01$ ,  $d_F/\lambda_L = 0.005$ , and  $R/\lambda_L = 3$  in the cases of the exponential, domain wall and linear anzats.

If the function  $\bar{\theta}(x)$  decays at  $x \rightarrow \infty$  faster than  $1/x^3$ , the expression (12) determines the supercurrent at  $r \ll r_\lambda$  only. Then at distances  $r \gg r_\lambda \gg R$  the asymptotic behavior of the supercurrent is given as (cf. Eq. (11)),

$$J_\varphi = 12c_2 M_s \frac{d_F \lambda R^2}{r^4}, \quad r_\lambda \ll r. \quad (13)$$

The length scale  $r_\lambda$  can be estimated from the condition  $|\bar{\theta}(r_\lambda/R)|^2 \sim \lambda R^3/r_\lambda^4$ . In the case of the exponential ansatz one finds  $r_\lambda \sim R \ln(R/\lambda) \gg R$ .

## B. The case of the linear ansatz

In the case of the linear ansatz the expression (7) for the function  $g(y)$  should be modified in order to have continuous solution for  $A_\varphi$  at  $r = R$ ,  $g(y) \rightarrow g_L(y)$ ,

$$g_L(y) = y \int_0^1 dx x J_0(yx) \left[ \cos(\pi x) + \frac{4}{\pi^2} \right] = g(y) + \delta g(y). \quad (14)$$

Here the function  $g(y)$  is given by Eq. (7) and  $\delta g(y) = -(1 - 4/\pi^2)J_1(y)$ . Therefore, the function  $g_L(y)$  has the following asymptotic behavior,

$$g_L(y) = \begin{cases} \frac{\pi^2 - 6}{2\pi^4} y^3 & , \quad y \ll 1, \\ \frac{\pi^2 - 4}{\pi^2} \frac{\sqrt{2} \cos(y + \pi/4)}{\sqrt{\pi y}} & , \quad y \gg 1. \end{cases} \quad (15)$$

We note that the abrupt change of  $\theta(r)$  at  $r = R$  results in oscillating behavior of  $g(y)$  at  $y \gg 1$ . The dependence of the function  $g_L(y)$  on  $y$  is shown in Fig. 2.

With the help of Eqs. (8) and (15), we obtain the following results for the asymptotic behavior of the su-

percurrent in the case of  $R \ll \lambda$  (see Appendix A),

$$J_\varphi = \frac{M_s d_F}{4\lambda} \begin{cases} (\pi \text{Si}(\pi) - 1 + 4/\pi^2)r/R, & r \ll R, \\ -3(\pi^2 - 6)R^4/(\pi^4 r^4), & R \ll r \ll \lambda, \\ -180(\pi^2 - 6)R^4 \lambda^2/(\pi^4 r^6), & \lambda \ll r. \end{cases} \quad (16)$$

Here  $\text{Si}(z)$  stands for the sine integral. We note that in the case of the linear ansatz the supercurrent decays at  $r \gg R$  faster than in the case of smooth skyrmion profile. This occurs due to the fact that the contribution to the current from  $\delta g(y)$  cancels the leading contributions from  $g(y)$ . This occurs since  $c_1 = (\pi^2 - 4)/(2\pi^2)$ . As in the case of smooth skyrmion profile, Eq. (16) suggests non-monotonous behavior of  $J_\varphi$  with  $r$ . There should be the maximum and the minimum in the supercurrent at the distances of the order of the skyrmion size  $R$ . Contrary to the case of smooth skyrmion profile, Eq. (16) describes asymptotic behavior of the smooth part of the supercurrent only. On the top of the monotonic dependence there is also weak oscillating contribution to  $J_\varphi$  with the typical length scale of the order of  $R$  as shown in Fig. 3. This oscillating contribution is the consequence of the abrupt boundary of the skyrmion configuration.

The dependence  $J_\varphi(r)$  in the case of large skyrmion size,  $R \gg \lambda$ , is more intricate. The supercurrent is given as the sum of the contribution discussed above for the case of the smooth skyrmion profile, cf. Eqs. (12) and (13), and the contribution due to  $\delta g(y)$ . At short distance,  $r \ll R$ , we find (see Appendix A),

$$J_\varphi = \frac{\pi^2 M_s d_F r}{R^2} \left( 1 - 3 \frac{\pi^2 - 4}{\pi^4} \frac{\lambda}{R} \right). \quad (17)$$

In the case of the long distance,  $r \gg R$  the supercurrent is given as

$$J_\varphi = -45 \frac{\pi^2 - 6}{\pi^4} \frac{M_s d_F \lambda R^4}{r^6}. \quad (18)$$

We note that in the case of the linear ansatz the supercurrent is stronger suppressed at  $r \gg R$  than in the case of a smooth skyrmion profile.

### III. INTERACTION ENERGY BETWEEN SKYRMION AND PEARL VORTEX

As above we focus on the case of a thin ( $d_S \ll \lambda_L$ ) superconducting film with a superconducting vortex situated at the distance  $a$  from the center of the Néel-type skyrmion (see Fig. 1). In order to compensate the magnetic flux carried by the vortex we assume that there exists anti-vortex located far away from the skyrmion-vortex pair. The free energy of this system, including the magnetic energy of the skyrmion can be written as

$$\mathcal{F} = \mathcal{F}_{\text{Sk}} + \mathcal{F}_V + \mathcal{F}_{\bar{V}} + \mathcal{F}_{\text{Sk}-V} + \mathcal{F}_{\text{Sk}-\bar{V}} + \mathcal{F}_{V-\bar{V}}. \quad (19)$$

Here  $\mathcal{F}_{\text{Sk}}$  denotes the magnetic free energy of the isolated chiral ferromagnet that leads to the appearance of the

Néel-type skyrmion (see its explicit form in the next section).  $\mathcal{F}_V$  and  $\mathcal{F}_{\bar{V}}$  are the free energies of the isolated superconducting vortex and anti-vortex, respectively. The electromagnetic interaction between the skyrmion and the vortex is described by the following free energy,

$$\mathcal{F}_{\text{Sk}-V} = \frac{1}{4\pi} \int d^3r \left( \mathbf{B}_{\text{Sk}} \mathbf{B}_V + \lambda_L^2 (\nabla \times \mathbf{B}_{\text{Sk}}) (\nabla \times \mathbf{B}_V) \right. \\ \left. \times \Theta(-z) \Theta(z + d_s) - 4\pi \mathbf{M}_{\text{Sk}} \mathbf{B}_V \right), \quad (20)$$

where  $\mathbf{B}_V = \nabla \times \mathbf{A}_V$  and  $\mathbf{B}_{\text{Sk}} = \nabla \times \mathbf{A}_{\text{Sk}}$  are the magnetic fields generated by the vortex and the skyrmion, respectively. We note that the first two terms in the right hand side of the expression for  $\mathcal{F}_{\text{Sk}-V}$  compensate each other in virtue of Eq. (2). Therefore, the distribution of the supercurrent does not influence the interaction energy between the skyrmion and the vortex. In what follows, we shall neglect the free energies of the interaction of the anti-vortex with the skyrmion,  $\mathcal{F}_{\text{Sk}-\bar{V}}$ , and with the vortex,  $\mathcal{F}_{V-\bar{V}}$ .

The magnetic field of the superconducting vortex in a thin film,  $d_S \ll \lambda_L$ , can be written in a standard form [28],

$$\mathbf{B}_V = \phi_0 \text{sgn}(z) \nabla \int \frac{d^2\mathbf{q}}{(2\pi)^2} \frac{e^{-q|z|+i\mathbf{q}(\mathbf{r}-\mathbf{a})}}{q(1+2q\lambda)}. \quad (21)$$

Here  $\phi_0 = hc/2e$  is the flux quantum,  $\mathbf{a}$  is the coordinate vector of the vortex center with respect to the skyrmion center. Since  $\mathcal{F}_{\text{Sk}-V}$  should depend on the distance  $a$  between the skyrmion and the vortex only, we can average the magnetic field  $\mathbf{B}_V$  over directions of the vector  $\mathbf{a}$ . This procedure implies that

$$\mathbf{B}_V \rightarrow -\phi_0 \int_0^\infty \frac{dq}{2\pi} \frac{q e^{-q|z|}}{1+2q\lambda} J_0(qa) \left[ \text{sgn}(z) J_1(qr) \mathbf{e}_r \right. \\ \left. + J_0(qr) \mathbf{e}_z \right]. \quad (22)$$

The free energy of the Pearl vortex (as well as anti-vortex) in a thin superconducting film is given by [27]

$$\mathcal{F}_V = \mathcal{F}_{\bar{V}} = \frac{\phi_0^2}{16\pi^2 \lambda} \ln \frac{\lambda}{\xi}, \quad (23)$$

where the superconducting coherence length is assumed to be much shorter than the Pearl length,  $\xi \ll \lambda$ .

Using Eqs. (1) and (22), we express the interaction part of the free energy as

$$\mathcal{F}_{\text{Sk}-V} = M_s \phi_0 d_F + M_s \phi_0 \int_0^\infty dq \frac{1 - e^{-qd_F}}{q(1+2q\lambda)} J_0(qa) \\ \times \int_0^\infty dr r \left[ \eta q + \theta'(r) \right] J_1(qr) \sin \theta(r). \quad (24)$$

We note that the first term in the right hand side of Eq. (24) corresponds to the homogeneous magnetization of the ferromagnetic film.

Below we analyse general expression (24) in the case of a thin ferromagnetic film,  $d_F \ll R$ . Then we find

$$\frac{\mathcal{F}_{\text{Sk-V}}}{M_s \phi_0 d_F} = 1 + \int_0^\infty dy \frac{J_0(ya/R)}{(1+2y\lambda/R)} \int_0^\infty dx x \left[ \eta y + \bar{\theta}'(x) \right] \times J_1(yx) \sin \bar{\theta}(x). \quad (25)$$

As in the case of the supercurrent, we start from the case of a skyrmion of size  $R \ll \lambda$ . Neglecting unity with respect to  $2y\lambda/R$  in the denominator of the integrand in the right hand side of Eq. (25), we obtain the following asymptotic expression for the interaction free energy at short distances,  $a \ll \lambda$ , (see Appendix B)

$$\frac{\mathcal{F}_{\text{Sk-V}}}{M_s \phi_0 d_F} = 1 + \frac{R}{2\lambda} f_\eta \left( \frac{a}{R} \right), \quad (26)$$

where the function  $f_\eta(z)$  has the following asymptotic behavior

$$f_\eta(z) = \begin{cases} \eta b_0 - 4c_1 + (2c_{-1} + \eta \bar{\theta}'(0)) z^2/2, & z \ll 1, \\ -c_2/z, & z \gg 1. \end{cases} \quad (27)$$

Here we introduced the numerical constants,

$$b_k = \int_0^\infty dx x^k \sin \bar{\theta}(x), \quad k = -1, 0, 1, \dots \quad (28)$$

At very long distances,  $a \gg \lambda$ , the free energy of interaction between the skyrmion and the vortex becomes (see Appendix B),

$$\frac{\mathcal{F}_{\text{Sk-V}}}{M_s \phi_0 d_F} = 1 - \frac{4c_2 R^2 \lambda}{a^3}. \quad (29)$$

We emphasize that at long distances  $a \gg R$   $\mathcal{F}_{\text{Sk-V}}$  becomes insensitive to chirality of the Néel skyrmion. The coefficient  $c_{-1}$  is typically positive whereas  $\bar{\theta}'(0)$  is negative, therefore the interaction free energy may decrease with increase of  $a$  for  $\eta = +1$ . Since the ratio  $\mathcal{F}_{\text{Sk-V}}/(M_s \phi_0 d_F)$  tends to unity at  $a \rightarrow \infty$  irrespective of chirality, one can expect the existence of the minimum of  $\mathcal{F}_{\text{Sk-V}}$  at some non-zero value of the distance  $a$ . This situation is realized for the exponential ansatz. In the case of 360-degree domain wall ansatz with  $\eta = +1$  the nontrivial minimum exists for  $\delta/R \gtrsim 0.64$  only.

Next we consider the opposite case of the skyrmion with the size much larger than the size of the Pearl vortex,  $R \gg \lambda$ . The interaction free energy can be written as a series in powers of  $\lambda/R$  (see Appendix B),

$$\frac{\mathcal{F}_{\text{Sk-V}}}{M_s \phi_0 d_F} = 1 + h_{\eta,0} \left( \frac{a}{R} \right) + \frac{\lambda}{R} h_{\eta,1} \left( \frac{a}{R} \right) + \dots \quad (30)$$

The function  $h_{\eta,0}$  that determines the magnitude of the interaction free energy has the following asymptotic behavior (see Appendix B),

$$h_{\eta,0}(z) = \eta b_{-1} - 2 + \left[ \frac{3}{4} \eta \bar{\theta}''(0) \ln z + \bar{\theta}'^2(0) + \eta \beta_0 \right] \frac{z^2}{2}, \quad (31)$$

at  $z \ll 1$ , and

$$h_{\eta,0}(z) = -\frac{\eta b_2}{2z^3}, \quad z \gg 1. \quad (32)$$

Here the parameter  $\beta_0$  is given by the following lengthy expression,

$$\beta_0 = \frac{3}{2} \bar{\theta}'(0) + \bar{\theta}''(0) \left[ \frac{7}{4} - \frac{3(1+2G)}{2\pi} - \frac{6}{\pi} \int_0^1 \frac{dx}{x^3} \left( K(x^2) - \frac{\pi}{2} - \frac{\pi x^2}{8} \right) \right] + \frac{3}{2} \int_1^\infty dx \frac{\sin \bar{\theta}(x)}{x^3} + \frac{3}{2} \int_0^1 dx \left[ \frac{\sin \bar{\theta}(x)}{x^3} + \frac{\bar{\theta}'(0)}{x^2} + \frac{\bar{\theta}''(0)}{2x} \right], \quad (33)$$

where  $G \approx 0.916$  denotes the Catalan's constant and  $K(x)$  stands for the complete elliptic integral of the first kind. The function  $h_{\eta,1}(z)$  that determines the dependence on distance of the subleading contribution to  $\mathcal{F}_{\text{Sk-V}}$  has the following asymptotic behavior (see Appendix B),

$$h_{\eta,1}(z) = 4(2c_{-1} + \eta \bar{\theta}'(0)) + 3\eta \bar{\theta}''(0)z - \left[ \frac{9}{4} \bar{\theta}'(0) \bar{\theta}''(0) \ln z + \frac{4}{3} \eta (\bar{\theta}'^3(0) - \bar{\theta}'''(0)) - \beta_1 \right] z^2, \quad z \ll 1, \quad (34)$$

and

$$h_{\eta,1}(z) = -\frac{4c_2}{z^3}, \quad z \gg 1. \quad (35)$$

Here the parameter  $\beta_1$  is given as

$$\begin{aligned} \beta_1 = & \frac{9}{2\pi} (1+2G) \bar{\theta}'(0) \bar{\theta}''(0) - \frac{1}{2} \int_1^\infty \frac{dx}{x^3} \partial_x (x \bar{\theta}'(x) \sin \bar{\theta}(x)) \\ & - \frac{1}{2} \int_0^1 \frac{dx}{x^3} \partial_x (x \bar{\theta}'(x) \sin \bar{\theta}(x) + \bar{\theta}'^2(0)x^2 + \frac{3}{2} \bar{\theta}'(0) \bar{\theta}''(0)x^3) \\ & + \frac{18}{\pi} \bar{\theta}'(0) \bar{\theta}''(0) \int_0^1 \frac{dx}{x^3} \left[ K(x^2) - \frac{\pi}{2} - \frac{\pi x^2}{8} \right] \\ & + \bar{\theta}'^2(0) - \frac{9}{2} \bar{\theta}'(0) \bar{\theta}''(0). \end{aligned} \quad (36)$$

We mention two discrepancies with the case of a skyrmion of a small radius. At first, the short distance behavior of the interaction free energy in the case of

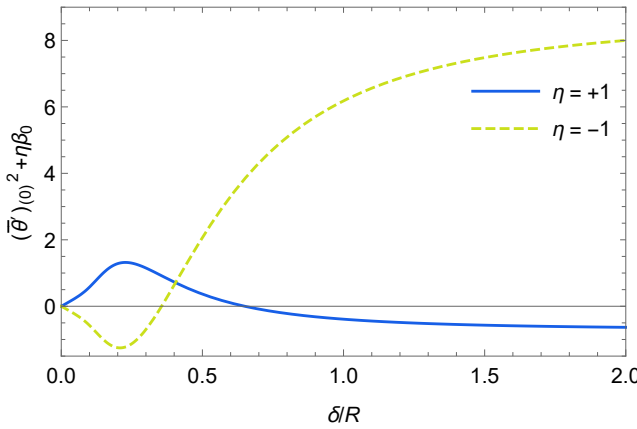


FIG. 4. The dependence of  $\bar{\theta}''(0) + \eta\beta_0$  on  $\delta/R$  (see text).

$R \gg \lambda$  is not parabolic generically, see Eq. (31). Secondly, the asymptotic behavior of  $\mathcal{F}_{\text{Sk-V}}$  at  $a \gg R$  depends on the skyrmion's chirality.

Provided  $\bar{\theta}''(0) > 0$ , the analytic results (31)–(32), suggest the existence of the global minimum of  $\mathcal{F}_{\text{Sk-V}}$  at a certain non-zero distance  $a$  in the case of positive skyrmion's chirality  $\eta = +1$ . For negative chirality,  $\eta = -1$ , the minimum of the interaction free energy is situated at  $a = 0$ . Interestingly, the 360-degree domain wall ansatz is special since  $\bar{\theta}''(0) = 0$ . Thus, for the 360-degree domain wall ansatz the existence of the minimum in  $\mathcal{F}_{\text{Sk-V}}$  is controlled by the sign of the term in the second line of Eq. (33). The dependence of this coefficient on the ratio  $\delta/R$  for both chiralities is shown in Fig. 4. For  $\delta \gtrsim 0.63R$  ( $\delta \lesssim 0.36R$ ) the interaction free energy,  $\mathcal{F}_{\text{Sk-V}}$ , has the minimum at nonzero value of  $a$  for the case of positive (negative) chirality,  $\eta = +1$  ( $\eta = -1$ ).

In Figs. 5 and 6 we show the behavior of the interaction free energy as a function of  $a/R$  for both chiralities,  $\eta = \pm 1$  and for the skyrmion radius equal to the Pearl length. As one can see, for positive chirality,  $\eta = +1$ , the minimum of  $\mathcal{F}_{\text{Sk-V}}$  is reached at nonzero value of the distance  $a$ .

#### IV. THE EFFECT OF THE PEARL VORTEX ON THE SKYRMION

The magnetic free energy of the chiral ferromagnetic film is given by [1]

$$\mathcal{F}_{\text{magn}}[\mathbf{m}] = d_F \int d^2\mathbf{r} \left\{ A(\nabla \mathbf{m})^2 + K(1 - m_z^2) + D[m_z \nabla \cdot \mathbf{m} - (\mathbf{m} \cdot \nabla)m_z] \right\}. \quad (37)$$

Here  $\mathbf{m}(\mathbf{r})$  denotes the unit vector of magnetization direction,  $A > 0$  stands for the exchange constant,  $D$  is the Dzyaloshinskii–Moriya interaction, and  $K > 0$  denotes the perpendicular anisotropy constant. The magnetic free energy is normalized in such a way that  $\mathcal{F}_{\text{magn}}$

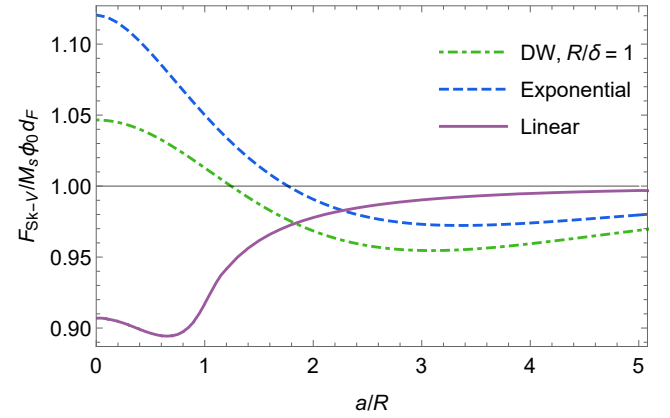


FIG. 5. The dependence of the normalized interaction free energy,  $\mathcal{F}_{\text{Sk-V}}$ , on  $a/R$  for the chirality  $\eta = +1$ . The ratio of the skyrmion radius and the Pearl length is unity,  $\lambda/R = 1$  (see text).

is zero for the ferromagnetic state,  $m_z = 1$ . Substituting  $\mathbf{m} = \mathbf{m}_{\text{Sk}} = \mathbf{M}_{\text{Sk}}/M_s$ , see Eq. (1), into Eq. (37), we find

$$\begin{aligned} \mathcal{F}_{\text{Sk}} \equiv \mathcal{F}_{\text{magn}}[\mathbf{m}_{\text{Sk}}] = 2\pi d_F \int_0^\infty dr r \left\{ A \left[ \bar{\theta}''(r) + \frac{\sin^2 \theta(r)}{r^2} \right] \right. \\ \left. + D\eta \left[ \bar{\theta}'(r) + \frac{\sin(2\theta(r))}{2r} \right] + K \sin^2 \theta(r) \right\}. \end{aligned} \quad (38)$$

Assuming a scaling form of the skyrmion profile,  $\theta(r) = \bar{\theta}(r/R)$ , we obtain

$$\mathcal{F}_{\text{Sk}} = d_F \left( \alpha_A A - \alpha_D \eta DR + \alpha_K KR^2/2 \right), \quad (39)$$

where

$$\begin{aligned} \alpha_A &= 2\pi \int_0^\infty dx x \left[ \bar{\theta}''(x) + \frac{\sin^2 \bar{\theta}(x)}{x^2} \right], \\ \alpha_D &= -2\pi \int_0^\infty dx x \left[ \bar{\theta}'(x) + \frac{\sin(2\bar{\theta}(x))}{2x} \right], \\ \alpha_K &= 4\pi \int_0^\infty dx x \sin^2 \bar{\theta}(x). \end{aligned} \quad (40)$$

We note that  $\alpha_{A,D,K}$  are positive constants in the case of the linear and exponential ansatz and are positive functions of the parameter  $R/\delta$  in the case of the 360-degree domain wall ansatz. Minimizing  $\mathcal{F}_{\text{Sk}}$  with respect to  $R$ , one can find the optimal radius of the skyrmion

$$R_0 = \alpha_D |D| / (\alpha_K K) \quad (41)$$

and the chirality  $\eta = \text{sgn } D$ . We note that the existence of a skyrmion in a chiral ferromagnetic film is possible under the following condition,

$$\alpha_A A < \alpha_K KR_0^2/2. \quad (42)$$

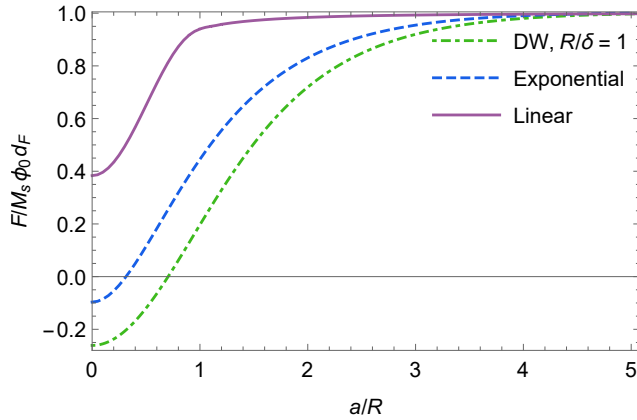


FIG. 6. The dependence of the normalized interaction free energy,  $\mathcal{F}_{\text{Sk-V}}$ , on  $a/R$  for the chirality  $\eta = -1$ . The ratio of the skyrmion radius and the Pearl length is unity,  $\lambda/R = 1$  (see text).

In order to simplify the presentation, we shall start our considerations below from the cases of the linear and exponential ansatz. In the presence of vortex anti-vortex pair the skyrmion radius is obtained by minimization of  $\mathcal{F}_{\text{Sk}} + \mathcal{F}_{\text{Sk-V}}$  with respect to  $R$  and  $a$ . Let us start from the case of a skyrmion of small radius,  $R_* \ll \lambda$ . For the negative chirality the optimal distance between the skyrmion and the vortex is zero. Therefore, as it follows from Eqs. (26) and (39), for  $\eta = -1$  the interaction between skyrmion and vortex results in increase of the skyrmion radius,

$$R_* = R_0 + (2c_1 + b_0/2)\ell_K^2/\lambda. \quad (43)$$

Here  $\ell_K = \sqrt{M_s \phi_0 / (\alpha_K K)}$  is the length scale associated with the anisotropy energy. In the case of the positive chirality the optimal distance between the vortex and the skyrmion is proportional to the skyrmion radius,  $a_0 = \zeta_0 R$ , see Eq. (26). Interestingly, we find that in the case of  $\eta = +1$  the skyrmion radius is also enlarged due to interaction with the vortex,

$$R_* = R_0 - f_{+1}(\zeta_0)\ell_K^2/(2\lambda). \quad (44)$$

We note that  $f_{+1}(\zeta_0) < 0$ . The results (43) and (44) are applicable for  $\lambda \gg \max\{R_0, \ell_K\}$ . In Table I we present estimates of  $R_*$  for several ferromagnet structures. As one can see from the Table I, the magnitude of the ratio  $R_*/R_0$  depends on a form of the ansatz for skyrmion profile. For some materials the skyrmion radius can be enhanced by 4 times.

In order a vortex-anti-vortex pair can be spontaneously generated in the presence of a skyrmion the total free energy (19) should be negative. This implies the following inequality,

$$\alpha_A A - \frac{\alpha_K K R_*^2}{2} + \alpha_K K \ell_K^2 + \frac{\phi_0^2}{8\pi^2 \lambda d_F} \ln \frac{\lambda}{\xi} < 0. \quad (45)$$

Since  $R_*$  is larger than  $R_0$  this inequality can be fulfilled provided the condition (42) holds. We note that then the radius of the skyrmion should satisfy  $\lambda \gg R_0 \gg \ell_K$ . In particular, the vortex-anti-vortex pair cannot be generated spontaneously in the absence of the Dzyaloshinskii-Moriya interaction, i.e. at  $D = 0$ . Indeed, in the latter case  $R_* \ll \ell_K$  and the left hand side of the inequality (45) is positive. In fact, there is a minimal value of the Dzyaloshinskii-Moriya interaction at which the spontaneous generation of a vortex-anti-vortex pair is possible,

$$|D| > \left[ \frac{2\alpha_K K}{\alpha_D^2} \left( \alpha_A A + \alpha_K K \ell_K^2 + \frac{\phi_0^2 \ln(\lambda/\xi)}{8\pi^2 \lambda d_F} \right) \right]^{1/2} + f_{\eta}(\zeta_0) \frac{\alpha_K K \ell_K^2}{2\alpha_D \lambda}. \quad (46)$$

Now let us assume that the skyrmion radius is large,  $R \gg \lambda$ . Then, Eqs. (30) and (39) result in the following equation for the skyrmion radius modified by the interaction with the vortex,

$$\frac{R_*^3}{R_0^3} - \frac{R_*^2}{R_0^2} = h_{\eta,1}(\zeta_0) \frac{\lambda \ell_K^2}{R_0^3}. \quad (47)$$

For negative chirality,  $\eta = -1$ , the optimal distance between the skyrmion and the vortex is zero,  $\zeta_0 = 0$ . We note that  $h_{-1,1}(0) = 4[2c_{-1} - \bar{\theta}'(0)] > 0$ , see Eq. (34). For positive chirality,  $\eta = +1$ , the interaction between skyrmion and vortex has the minimum at finite distance,  $\zeta_0 \neq 0$ . However, as one can check (see Eq. (B5)),  $h_{+1,1}(\zeta_0) > 0$ . Therefore, for both chiralities the skyrmion-vortex interaction leads to increase of the skyrmion radius,

$$R_* = R_0 (1 + X^{-1/3} + X^{1/3})/3, \quad (48)$$

where

$$X = 1 + \frac{27u}{2} + 6\sqrt{3u + 81u^2}, \quad u = h_{\eta,1}(\zeta_0) \frac{\lambda \ell_K^2}{4R_0^3}. \quad (49)$$

We note that for  $R_0 \ll (\lambda \ell_K^2)^{1/3}$  and  $\ell_K \gg \lambda$  the skyrmion radius is parametrically enhanced,  $R_* \sim (\lambda \ell_K^2)^{1/3} \gg R_0$ . For  $R_0 \gg (\lambda \ell_K^2)^{1/3}$ , the radius of the skyrmion is only slightly increased,  $R_* \sim R_0$ . In this case Eq. (48) holds under assumption  $R_0 \gg \lambda$ .

A spontaneous generation of the vortex-anti-vortex pair requires the negative total free energy (19),

$$\alpha_A A - \frac{\alpha_K K R_*^2}{2} + \alpha_K K \ell_K^2 \left[ 1 + h_{\eta,0}(\zeta_0) + 2h_{\eta,1}(\zeta_0) \frac{\lambda}{R_*} \right] + \frac{\phi_0^2}{8\pi^2 \lambda d_F} \ln \frac{\lambda}{\xi} < 0. \quad (50)$$

Since  $R_* > R_0$  the above inequality can be satisfied provided the condition (42) holds. However, it can occur only for sufficiently large bare skyrmion radius,  $R_0 \gg \lambda \gg \ell_K$ . In the case  $\ell_K \gg R_0 \gg \lambda$  the skyrmion radius becomes  $R_* \sim (\lambda \ell_K^2)^{1/3} \ll \ell_K$ . Therefore, the

TABLE I. The parameters  $M_s, A, K_u$ , and  $D$  for a number of thin chiral ferromagnet films. The estimates for the a bare ( $R_0$ ) and effective ( $R_*$ ) skyrmion radii and an anisotropic scale  $\ell_K$  for the linear (lin) and exponential (exp) ansatz are given. In order to obtain the estimate for  $R_*$  we choose  $\lambda = 100$  nm.

	PtCoPt [29, 30]	IrCoPt [31]	PtCoNiCo [32]	PdFeIr [33, 34]
Saturation magnetization $M_s$ ( $10^3$ A/m)	580	956	600	1100
Exchange constant $A$ ( $10^{-12}$ J/m)	15	10	20	2.0
Anisotropy constant $K_u$ ( $10^6$ J/m $^3$ )	0.7	0.717	0.6	2.5
DMI parameter $D$ ( $10^{-3}$ J/m $^2$ )	+3	+1.6	+3	+3.9
Bare radius (lin/exp) $R_0$ ( $10^{-9}$ m)	13/4	7.0/2.1	20/5	5.0/1.5
Skyrmion radius (lin/exp) $R_*$ ( $10^{-9}$ m)	26/5.5	28/4.4	30/6	12/2.3
Anisotropy scale (lin/exp) $\ell_K$ ( $10^{-9}$ m)	80/40	100/47	90/40	60/26

negative term  $-\alpha_K K R_*^2/2$  is much smaller than the positive term  $\alpha_K K \ell_K^2$  and, consequently, spontaneous generation of vortex–anti-vortex pair is not possible.

In the case of the 360-degree domain wall ansatz Eqs. (43), (44), and (47) remain valid. However, the value of  $\zeta_0$  depends on the ratio  $R_*/\delta$ . The latter is determined from the minimum of the total free energy with respect to  $\delta$ . The corresponding analysis can be performed numerically. As one can check, the following inequalities hold  $f_\eta(\zeta_0) < 0$  and  $h_{\eta,1}(\zeta_0) > 0$ . These inequalities imply that the skyrmion radius increases always in the presence of a vortex–anti-vortex pair.

## V. SUMMARY AND CONCLUSIONS

To summarize, we have studied an interaction of a Néel-type skyrmion and a vortex–anti-vortex pair due to stray fields in a chiral ferromagnet–superconductor heterostructure. We computed the supercurrent in a superconducting film induced by a skyrmion. For thin ferromagnet and superconductor films we found that the supercurrent has the maximum at the distance from the center of a skyrmion that is of the order of the skyrmion radius. It is worthwhile to mention that the supercurrent is sensitive to a profile of the skyrmion. For example, in the case of smooth profiles (exponential and domain wall ansatzes), the supercurrent decays monotonously at large distances from the skyrmion center. For the case of a linear profile, there are decaying oscillations of the supercurrent at large distances due to discontinuity in  $\theta'(r)$  at  $r = R$ . Therefore, measurements of dependence of the supercurrent on distance can allow one to extract information on the profile of a skyrmion. We mention that the behavior of the supercurrent with a distance from the center of the skyrmion is qualitatively similar to the behavior of the supercurrent induced in a thin superconducting film by a Bloch domain wall in a ferromagnetic film [26]. The radius of the skyrmion plays the same role as the width of a domain wall.

We have also computed the energy of interaction between a Néel-type skyrmion and a Pearl vortex. We found that the interaction with a Pearl vortex is sensi-

tive to the skyrmion chirality. In the case of a skyrmion with negative chirality, typically, it is more energetically favourable for a vortex to be attracted to the skyrmion center. This occurs in the cases of linear and exponential skyrmion profiles and for a domain wall ansatz with  $\delta \gtrsim 0.36R$ . In the case of positive skyrmion chirality a vortex is situated at a finite distance (of the order of skyrmion radius) from the center of the skyrmion. This happens for linear and exponential profiles and in the case of domain wall ansatz with  $\delta \gtrsim 0.63R$ .

It is worthwhile to mention that in the case of a Bloch-type skyrmion it is always energetically favorable for a vortex to settle at the center of the skyrmion [21]. Such a behavior is related with the absence of the radial component of magnetization in a Bloch-type skyrmion. Therefore, the Bloch-type skyrmion interacts with the  $z$ -component of the magnetic field of a Pearl vortex only. This leads to the absence of terms proportional to the chirality  $\eta$  in Eqs. (27) and (31). As a result, the function  $f_\eta(z)$  and  $h_{\eta,0}(z)$  behave as increasing parabolas at  $z \ll 1$ . Such a behavior implies the minimum of the interaction free energy at zero distance between the center of the Bloch-type skyrmion and the Pearl vortex.

The fact that it is energetically favourable for a Pearl vortex to take place at a finite distance from the center of a Néel-type skyrmion can have interesting implications for skyrmion lattices [35] and dynamics of skyrmions [22] in superconductor – ferromagnet heterostructures [36].

We have investigated how a Pearl vortex affects a Néel-type skyrmion due to their mutual interaction. We found that a vortex–anti-vortex pair leads to an increase of the radius of the Néel-type skyrmion. We note that this result can be contrasted with the case of a Bloch-type skyrmion for which a vortex–anti-vortex pair can either increase or decrease the skyrmion radius [21]. It is also possible that a vortex–anti-vortex pair will be spontaneously generated in the presence of a Néel-type skyrmion provided the skyrmion radius and Pearl penetration length are large enough in comparison with the length associated with the anisotropy energy in a chiral ferromagnet,  $\lambda, R_0 \gg \ell_K$ . In the opposite case of small bare skyrmion radius,  $R_0 \ll \ell_K$ , spontaneous generation of a vortex–anti-vortex pair is not pos-

sible. Unfortunately, the relation,  $R_0 \ll \ell_K$ , typically holds in a chiral ferromagnets (see Table I). However, for  $R_0 \ll (\lambda\ell_K^2)^{1/3} \ll \ell_K$ , we predict that a vortex–anti-vortex pair existing in a superconducting film can substantially increase the skyrmion radius: it becomes equal to  $R_* \sim (\lambda\ell_K^2)^{1/3} \gg R_0$ . The typical values of  $R_0$ ,  $\ell_K$ , and  $R_*$  are listed in Table I. Abrupt increase of the skyrmion radius can be used as indication of appearance of vortex–anti-vortex pairs in superconducting films. It is an experimental challenge to detect enhancement of the skyrmion radius in a thin ferromagnet–superconductor heterostructure due to generation of vortex–anti-vortex pair in a superconducting film.

Finally, we mention that it would be interesting to generalize our results to the case of more exotic magnetic excitations, e.g. antiskyrmions, bimerons, biskyrmions, skyrmioniums, etc. [37]

## ACKNOWLEDGMENTS

The authors are grateful to M. Garst for useful comments. The work was funded in part by Russian Science Foundation under the grant No. 21-42-04410.

## Appendix A: Derivation of the asymptotic expressions for the supercurrent

In this Appendix we present some details of derivation of expressions for the supercurrent.

### 1. The case of a smooth skyrmion profile

We start from the case of the smooth skyrmion profile. According to Eq. (8) the supercurrent is determined by the function  $g(y)$ , see Eq. (7).

To find the asymptotic behavior of the function  $g(y)$  in the case of a small argument,  $y \ll 1$ , we approximate the Bessel function  $J_1(xy)$  by  $xy/2$  and find,

$$g(y) = -y/2 \int_0^\infty dx x^2 \bar{\theta}'(x) \sin \bar{\theta}(x) \simeq 2c_2 y, \quad y \ll 1. \quad (\text{A1})$$

Asymptotic expression at large arguments,  $y \gg 1$ , can be found in the following way. Changing the variable  $x$  to  $xy$  under the integral sign in the definition of the function  $g(y)$ , see Eq. (7), one can expand the function  $\theta$  in powers of  $1/y$ . Then, we obtain

$$g(y) = \lim_{\beta \rightarrow +0} \int_0^\infty dx J_1(x) e^{-\beta x} \left[ \bar{\theta}'(0) + \frac{3x}{2y} \bar{\theta}''(0) \right] \frac{\bar{\theta}'(0)x^2}{y^3} \simeq -9\bar{\theta}'(0)\bar{\theta}''(0)/(2y^4), \quad y \gg 1. \quad (\text{A2})$$

Equations (A1) and (A2) are equivalent to Eq. (9).

We will now present derivation of asymptotic expressions for the supercurrent in the case of a small skyrmion,  $R \ll \lambda$ . At the shortest distances to the center of a skyrmion, one can neglect unity in the denominator of the expression (8) and expand the Bessel function in series of  $r/R \ll 1$ . Then we retrieve,

$$J_\varphi = M_s \frac{d_F r}{4\lambda R} \int_0^\infty dy y g(y) \quad (\text{A3})$$

The integral  $\int_0^\infty dy y g(y)$  can be simplified with the help of the following identity  $y J_1(xy) = -\partial_x(J_0(xy))$ . Then, we obtain

$$\begin{aligned} \int_0^\infty dy y g(y) &= - \int_0^\infty dx x \bar{\theta}'(x) \sin \bar{\theta}(x) \int_0^\infty dy y J_1(xy) \\ &= 4c_{-1}. \end{aligned} \quad (\text{A4})$$

This results in  $J_\varphi = (M_s d_F / \lambda) r / R$  for  $r \ll R$ , cf. Eq. (11).

For the case of long distances,  $r \gg R$ , we rewrite the expression for the supercurrent in a more convenient way, raising the denominator into exponent by means of an additional integration,

$$J_\varphi = M_s \frac{d_F}{R} \int_0^\infty dy \int_0^\infty dt e^{-t(1+2y\lambda/R)} y g(y) J_1(yr/R). \quad (\text{A5})$$

Let us first consider the integration with respect to the  $y$  variable. Since for  $r/R \gg 1$  the integral over  $y$  is dominated by small values of  $y$ , we obtain

$$\begin{aligned} \int_0^\infty dy y e^{-2yt\lambda/R} J_1(xy) J_1(yr/R) &\simeq \frac{x}{2} \int_0^\infty dy y^2 e^{-y(2t\lambda/R)} \\ &\times J_1(yr/R) = \frac{x}{2} \frac{3(2\lambda t/r)}{[1 + (2\lambda t/r)^2]^{5/2}} \frac{R^3}{r^3}. \end{aligned} \quad (\text{A6})$$

Hence for the supercurrent we write

$$J_\varphi = 2c_2 M_s \frac{d_F R^2}{r^3} \int_0^\infty dt \frac{3(2\lambda t/r)e^{-t}}{[1 + (2\lambda t/r)^2]^{5/2}}. \quad (\text{A7})$$

In this integral form for the supercurrent, one can clearly figure out the behavior of  $J_\varphi(r)$  for  $r \ll \lambda$  and  $r \gg \lambda$ . For  $r \ll \lambda$  we can substitute  $e^{-t}$  by unity and, then, obtain  $J_\varphi = (M_s d_F / \lambda) (c_2 R^2 / r^2)$ , cf. Eq. (11). Otherwise, when  $r$  is much larger than  $\lambda$ , we neglect the term proportional to the small parameter  $\lambda/r$  in the denominator of (A7). Then, one gets  $J_\varphi = (M_s d_F / \lambda) (12c_2 \lambda^2 R^2 / r^4)$ , cf. Eq. (11).

Now we consider the case of large skyrmion  $R \gg \lambda$ . We start from the limit of short distances  $r \ll r_\lambda$ . In this regime we neglect the unity in the denominator

in the right hand side of Eq. (8). Using the identity  $\int_0^\infty dy y J_\alpha(xy) J_\alpha(zy) = \delta(x-z)/x$ , we find

$$\begin{aligned} J_\varphi &= -M_s \frac{d_F}{R} \int_0^\infty dx \bar{\theta}'(x) \sin \bar{\theta}(x) \delta(x - r/R) \\ &= -M_s \frac{d_F}{R} \bar{\theta}'(r/R) \sin \bar{\theta}(r/R), \quad r \ll r_\lambda. \end{aligned} \quad (\text{A8})$$

Equation (A8) is equivalent to Eq. (12). The asymptotic expression (13) for  $r \gg r_\lambda$  can be easily derived from Eq. (A6).

## 2. The case of the linear ansatz

Let us start from the case of  $R \ll \lambda$  and derive the asymptotic expression (16) for the supercurrent. At shortest distances,  $r \ll R$ , one writes similar to the case of the smooth profile,

$$J_\varphi = M_s \frac{d_F}{2\lambda} \int_0^\infty dy g_L(y) J_1(yr/R). \quad (\text{A9})$$

Since  $g_L(y) = g(y) + \delta g(y)$ , for the first contribution to  $J_\varphi$  we can use the expression (A4). While for the second term,  $\delta g(y) = -4c_2 J_1(y)$ , we apply the identity

$$\begin{aligned} \int_0^\infty dy J_1(y) J_1(yr/R) &= \frac{2R}{\pi r} [K(R^2/r^2) - E(R^2/r^2)] \\ &\simeq r/(2R) + O(r^3/R^3), \quad r \ll R. \end{aligned} \quad (\text{A10})$$

Here  $K(z)$  and  $E(z)$  denotes the complete elliptic integrals of the first and second kinds. Together, these two contributions give the final result, cf. Eq. (16),

$$J_\varphi = \left( \pi \text{Si}(\pi) - 1 + \frac{4}{\pi^2} \right) M_s \frac{d_F r}{4\lambda R}. \quad (\text{A11})$$

To find the behaviour of the superconducting current at large distances we use the method as described around Eq. (A6) above. The only difference is that instead of the expression for the smooth profile function  $g(y)$  we need to use the expression (14) for  $g_L(y)$ . Then, we retrieve,

$$\begin{aligned} \int_0^\infty dy y^2 e^{-2yt\lambda/R} J_0(xy) J_1(yr/R) &\simeq -\frac{x^2}{4} \int_0^\infty dy y^4 e^{-2yt\lambda/R} \\ &\times J_1(yr/R) = \frac{x^2 R^5}{4r^5} \frac{15(2\lambda t/r) (4(2\lambda t/r)^2 - 3)}{[1 + (2\lambda t/r)^2]^{9/2}}. \end{aligned} \quad (\text{A12})$$

This leads to the following approximate expression for the supercurrent,

$$J_\varphi = M_s \frac{d_F R^4}{r^5} \frac{6 - \pi^2}{2\pi^4} \int_0^\infty dt e^{-t} \frac{30\lambda t (4(2\lambda t/r)^2 - 3)}{r [1 + (2\lambda t/r)^2]^{9/2}}. \quad (\text{A13})$$

In the case of  $R \ll r \ll \lambda$ , the exponent  $e^{-t}$  in the right hand side of Eq. (A13) can be approximated by the unity. Then, we obtain, cf. Eq. (16),

$$J_\varphi = -\frac{3(\pi^2 - 6)}{4\pi^4} M_s \frac{d_F R^4}{\lambda r^4}. \quad (\text{A14})$$

In the limit of longest distances,  $r \gg \lambda$ , we neglect the terms  $(2\lambda t/r)^2$  in the numerator and denominator under the integral in Eq. (A13). Then, we find, cf. Eq. (16),

$$J_\varphi = -\frac{45(\pi^2 - 6)}{\pi^4} M_s \frac{d_F \lambda R^4}{r^6}. \quad (\text{A15})$$

Finally, we derive asymptotic expressions for the supercurrent for the case of a large skyrmion,  $R \gg \lambda$ . As it was explained in the main text, we are to compare the contributions from the term  $g(y)$ , given in (7), and from the  $\delta g(y) = -4c_2 J_1(y)$ . Let us start from the limit  $r \ll R$ . We can use Eq. (A8) for the asymptotic expression, corresponding to the contribution due to  $g(y)$ . In the case of the linear ansatz it reads  $(M_s d_F / R) \pi^2 (r/R)$ . In order to find the contribution due to the second term,  $\delta g(y)$ , we replace the Bessel function  $J_1(yr/R)$  by  $yr/(2R)$  and expand denominator in powers of  $y\lambda/R$ . Then, we find

$$\begin{aligned} -2c_2 \frac{r}{R} \lim_{\beta \rightarrow +0} \int_0^\infty dy e^{-\beta y} y J_1(y) \left[ 1 - \frac{2y\lambda}{R} + O\left(\frac{\lambda^2}{R^2}\right) \right] \\ \simeq -12c_2 \frac{\lambda r}{R^2}. \end{aligned} \quad (\text{A16})$$

Bringing these two contributions together, we retrieve, cf. Eq. (17),

$$J_\varphi = \frac{\pi^2 M_s d_F r}{R^2} \left( 1 - 3 \frac{\pi^2 - 4}{\pi^4} \frac{\lambda}{R} \right), \quad r \ll R. \quad (\text{A17})$$

For  $r \gg R \gg \lambda$  one can repeat derivation following Eqs. (A12) and (A13). Then one arrives eventually at the expression (A15).

## Appendix B: Derivation of the asymptotic expressions for the interaction energy

In this appendix we present some details of derivation of the asymptotic expressions for  $\mathcal{F}_{\text{Sk-V}}$ .

We start from the case of a small skyrmion and a large vortex,  $R \ll \lambda$ . In the regime of short distances,  $a \ll R$ , we can neglect the unity in comparison to the large parameter  $\lambda/R$  in the denominator under the integral sign in the right hand side of Eq. (25). Expanding the Bessel function  $J_0(ya/R)$  in series of  $ya/R$ , we obtain

$$\begin{aligned} \frac{\mathcal{F}_{\text{Sk-V}}}{M_s \phi_0 d_F} &\simeq 1 + \int_0^\infty dy \frac{1 - (a/R)^2 y^2/4}{2y\lambda/R} \int_0^\infty dx x [\eta y + \bar{\theta}'(x)] \\ &\times J_1(yx) \sin \bar{\theta}(x). \end{aligned} \quad (\text{B1})$$

This expression can be easily simplified to the form of Eq. (26).

For the intermediate distances,  $R \ll a \ll \lambda$ , one can simplify Eq. (25) by using the following identities,

$$\int_0^\infty dy J_0(yz) J_1(xy) = \Theta(x-z)/x, \quad (B2)$$

$$\begin{aligned} \int_0^\infty \frac{dy}{y} J_0(y) J_1(xy) &= \frac{2}{\pi x} \left[ E(x^2) - (1-x^2) K(x^2) \right] \\ &\times \Theta(1-x) + \frac{2}{\pi} E(x^{-2}) \Theta(x-1). \end{aligned} \quad (B3)$$

Here  $\Theta(x)$  denotes the Heaviside step function. After some simplifications, the expression for the interaction energy can be brought to the form of Eq. (26).

The case of the longest distances,  $a \gg \lambda$  can be studied in the following way. One can transform the expression in the denominator under the integral sign in the right hand side of Eq. (25) into the exponent with the help of an additional integration,  $1/(1+2y\lambda/R) = \int_0^\infty dt e^{-t(1+2y\lambda/R)}$ . Then expanding the Bessel function  $J_1(xy)$  in its argument to the lowest order, we derive Eq. (29).

Now let us consider the opposite case of large skyrmion radius,  $R \gg \lambda$ . Making in Eq. (25) expansion in powers of  $\lambda/R$ , we obtain Eq. (30) with the functions  $h_{\eta,0}(z)$  and  $h_{\eta,1}(z)$  that are given as

$$h_{\eta,0} = \int_0^\infty dx dy x J_0(yz) J_1(yx) [\eta y + \bar{\theta}'(x)] \sin \bar{\theta}(x) \quad (B4)$$

and

$$h_{\eta,1} = -2 \int_0^\infty dx dy xy J_0(yz) J_1(yx) [\eta y + \bar{\theta}'(x)] \sin \bar{\theta}(x). \quad (B5)$$

We shall start with the asymptotic behavior of the functions  $h_{\eta,0}(z)$  and  $h_{\eta,1}(z)$  at  $z \ll 1$ . Using the fol-

lowing identities  $y J_1(xy) = -d J_0(xy)/dx$ ,

$$\int_0^\infty dy y J_0(yz) J_0(xy) = \delta(x-z)/z, \quad (B6)$$

and Eq. (B2), we can simplify Eqs. (B4) and (B5) as follows

$$\begin{aligned} h_{\eta,0}(z) &= \cos \bar{\theta}(z) - 1 + \frac{2\eta}{\pi} \int_0^z \frac{dx}{z} \chi_0(x) K\left(\frac{x^2}{z^2}\right) \\ &+ \frac{2\eta}{\pi} \int_z^\infty \frac{dx}{x} \chi_0(x) K\left(\frac{z^2}{x^2}\right) \end{aligned} \quad (B7)$$

and

$$\begin{aligned} h_{\eta,1}(z) &= -2\eta \frac{\chi_0(z)}{z} - \frac{4}{\pi} \int_0^z \frac{dx}{z} \chi_1(x) K\left(\frac{x^2}{z^2}\right) \\ &- \frac{4}{\pi} \int_z^\infty \frac{dx}{x} \chi_1(x) K\left(\frac{z^2}{x^2}\right), \end{aligned} \quad (B8)$$

where  $\chi_0(x) = [x \sin \bar{\theta}(x)]'$  and  $\chi_1(x) = [x \bar{\theta}'(x) \sin \bar{\theta}(x)]'$ . Next we rewrite the integrals over the region  $x > z$  in the right hand side of Eqs. (B7) and (B8) in the following form,

$$\begin{aligned} \frac{2}{\pi} \int_z^\infty \frac{dx}{x} \chi_{0,1}(x) K\left(\frac{z^2}{x^2}\right) &= \int_z^\infty \frac{dx}{x} \chi_{0,1}(x) + \frac{z^2}{4} \int_z^\infty \frac{dx}{x^3} \chi_{0,1}(x) \\ &+ \frac{2}{\pi} \int_z^\infty \frac{dx}{x} \chi_{0,1}(x) \left[ K\left(\frac{z^2}{x^2}\right) - \left(\frac{\pi}{2} + \frac{\pi z^2}{8x^2}\right) \right]. \end{aligned} \quad (B9)$$

Written in this way, each of the terms converges at  $z \rightarrow 0$  and the asymptotic behaviour of  $h_{\eta,0}(z)$  and  $h_{\eta,1}(z)$  can be easily extracted. Then we reproduce Eqs. (31) and (34).

For large values of the argument,  $z \gg 1$ , it is enough to consider the term in Eqs. (B7) and (B8) which is proportional to the integral over the region  $x < z$ . We can also expand the complete elliptic function of the first kind as  $K(x^2/z^2) = \pi/2 + \pi x^2/(8z^2) + \dots$ . Then one can derive Eqs. (32) and (35).

---

[1] A. N. Bogdanov and D. Yablonskii, “Thermodynamically stable “vortices” in magnetically ordered crystals. The mixed state of magnets,” Sov. Phys. JETP **68**, 101 (1989).

[2] C. Back, V. Cros, H. Ebert, K. Everschor-Sitte, A. Fert, M. Garst, T. Ma, S. Mankovsky, T. L. Monchesky, M. Mostovoy, N. Nagaosa, S. S. P. Parkin, C. Pfleiderer, N. Reyren, A. Rosch, Y. Taguchi, Y. Tokura, K. von Bergmann, and J. Zang, “The 2020 skyrmionics roadmap,” J. Phys. D: Applied Phys. **53**, 363001 (2020).

[3] V. V. Ryazanov, V. A. Oboznov, A. S. Prokofiev, V. V. Bolginov, and A. K. Feofanov, “Superconductor-ferromagnet-superconductor  $\pi$ -junctions,” J. Low Temp. Phys. **136**, 385 (2004).

[4] I. F. Lyuksyutov and V. L. Pokrovsky, “Ferromagnet-superconductor hybrids,” Adv. Phys. **54**, 67 (2005).

[5] A. I. Buzdin, “Proximity effects in superconductor-ferromagnet heterostructures,” Rev. Mod. Phys. **77**, 935

(2005).

[6] F. S. Bergeret, A. F. Volkov, and K. B. Efetov, “Odd triplet superconductivity and related phenomena in superconductor-ferromagnet structures,” *Rev. Mod. Phys.* **77**, 1321 (2005).

[7] M. Eschrig, “Spin-polarized supercurrents for spintronics: A review of current progress,” *Rep. Prog. Phys.* **78**, 104501 (2015).

[8] S. S. Pershoguba, S. Nakosai, and A. V. Balatsky, “Skyrmion-induced bound states in a superconductor,” *Phys. Rev. B* **94**, 064513 (2016).

[9] K. Pöyhönen, T. Ojanen, A. Westström, S. S. Pershoguba, and A. V. Balatsky, “Skyrmion-induced bound states in a p-wave superconductor,” *Phys. Rev. B* **94**, 214509 (2016).

[10] W. Chen and A. P. Schnyder, “Majorana edge states in superconductor-noncollinear magnet interfaces,” *Phys. Rev. B* **92**, 214502 (2015).

[11] G. Yang, P. Stano, J. Klinovaja, and D. Loss, “Majorana bound states in magnetic skyrmions,” *Phys. Rev. B* **93**, 224505 (2016).

[12] U. Güngörbü, S. Sandhoefer, and A. A. Kovalev, “Stabilization and control of majorana bound states with elongated skyrmions,” *Phys. Rev. B* **97**, 115136 (2018).

[13] E. Mascot, S. Cocklin, S. Rachel, and D. K. Morr, “Dimensional tuning of majorana fermions and real space counting of the chern number,” *Phys. Rev. B* **100**, 184510 (2019).

[14] S. Rex, I. V. Gornyi, and A. D. Mirlin, “Majorana bound states in magnetic skyrmions imposed onto a superconductor,” *Phys. Rev. B* **100**, 064504 (2019).

[15] M. Garnier, A. Mesaros, and P. Simon, “Topological superconductivity with deformable magnetic skyrmions,” *Commun. Phys.* **2**, 126 (2019).

[16] S. Rex, I. V. Gornyi, and A. D. Mirlin, “Majorana modes in emergent-wire phases of helical and cycloidal magnet-superconductor hybrids,” *Phys. Rev. B* **102**, 224501 (2020).

[17] T. Yokoyama and J. Linder, “Josephson effect through magnetic skyrmions,” *Phys. Rev. B* **92**, 060503(R) (2015).

[18] V. L. Vadimov, M. V. Sapozhnikov, and A. S. Mel’nikov, “Magnetic skyrmions in ferromagnet-superconductor (f/s) heterostructures,” *Appl. Phys. Lett.* **113**, 032402 (2018).

[19] K. M. D. Hals, M. Schechter, and M. S. Rudner, “Composite topological excitations in ferromagnet-superconductor heterostructures,” *Phys. Rev. Lett.* **117**, 017001 (2016).

[20] J. Baumard, J. Cayssol, F. S. Bergeret, and A. Buzdin, “Generation of a superconducting vortex via Néel skyrmions,” *Phys. Rev. B* **99**, 014511 (2019).

[21] S. M. Dahir, A. F. Volkov, and I. M. Eremin, “Interaction of skyrmions and Pearl vortices in superconductor-chiral ferromagnet heterostructures,” *Phys. Rev. Lett.* **122**, 097001 (2019).

[22] R. M. Menezes, J. F. S. Neto, C. C. de Souza Silva, and M. V. Milošević, “Manipulation of magnetic skyrmions by superconducting vortices in ferromagnet-superconductor heterostructures,” *Phys. Rev. B* **100**, 014431 (2019).

[23] S. M. Dahir, A. F. Volkov, and I. M. Eremin, “Meissner currents induced by topological magnetic textures in hybrid superconductor/ferromagnet structures,” *Phys. Rev. B* **102**, 014503 (2020).

[24] Y. Kawaguchi, Y. Tanaka, and N. Nagaosa, “Skyrmionic magnetization configurations at chiral magnet/ferromagnet heterostructures,” *Phys. Rev. B* **93**, 064416 (2016).

[25] L.D. Landau and E.M. Lifshitz, *in the Course in Theoretical Physics, Vol. 8* (Pergamon Press, Oxford, 1984).

[26] I. S. Burmistrov and N. M. Chtchelkatchev, “Domain wall effects in ferromagnet-superconductor structures,” *Phys. Rev. B* **72**, 144520 (2005).

[27] J. Pearl, “Current distribution in superconducting films carrying quantized fluxoids,” *Appl. Phys. Lett.* **5**, 65 (1964).

[28] A. A. Abrikosov, *Fundamentals of the Theory of Metals* (North-Holland, Amsterdam, 1988).

[29] P. J. Metaxas, J. P. Jamet, A. Mougin, M. Cormier, J. Ferré, V. Baltz, B. Rodmacq, B. Dieny, and R. L. Stamps, “Creep and flow regimes of magnetic domain-wall motion in ultrathin Pt/Co/Pt films with perpendicular anisotropy,” *Phys. Rev. Lett.* **99**, 217208 (2007).

[30] J. Sampaio, V. Cros, S. Rohart, A. Thiaville, and A. Fert, “Nucleation, stability and current-induced motion of isolated magnetic skyrmions in nanostructures,” *Nat. Nanotechnol.* **8**, 839 (2013).

[31] C. Moreau-Luchaire, C. Moutafis, N. Reyren, J. Sampaio, C. A. F. Vaz, N. Van Horne, K. Bouzehouane, K. Garcia, C. Deranlot, P. Wernicke, P. Wohlhüter, J.-M. George, M. Weigand, J. Raabe, V. Cros, and A. Fert, “Additive interfacial chiral interaction in multilayers for stabilization of small individual skyrmions at room temperature,” *Nat. Nanotechnol.* **11**, 444 (2016).

[32] K.-S. Ryu, S.-H. Yang, L. Tomas, and S. S. P. Parkin, “Chiral spin torque arising from proximity-induced magnetization,” *Nat. Commun.* **5**, 3910 (2014).

[33] N. Romming, C. Hanneken, M. Menzel, J. E. Bickel, B. Wolter, K. von Bergmann, A. Kubetzka, and R. Wiesendanger, “Writing and deleting single magnetic skyrmions,” *Science* **341**, 636 (2013).

[34] N. Romming, A. Kubetzka, C. Hanneken, K. von Bergmann, and R. Wiesendanger, “Field-dependent size and shape of single magnetic skyrmions,” *Phys. Rev. Lett.* **114**, 177203 (2015).

[35] E. Balkind, A. Isidori, and M. Eschrig, “Magnetic skyrmion lattice by the Fourier transform method,” *Phys. Rev. B* **99**, 134446 (2019).

[36] to be published elsewhere.

[37] B. Göbel, I. Mertig, and O. A. Tretiakov, “Beyond skyrmions: Review and perspectives of alternative magnetic quasiparticles,” *Phys. Rep.* **895**, 1 (2021).